

# Direct evidence for cosmic-ray-induced correlated errors in superconducting qubit array

Xue-Gang Li,<sup>1,\*</sup> Jun-Hua Wang,<sup>1,\*</sup> Yao-Yao Jiang,<sup>1,2,3</sup> Guang-Ming Xue,<sup>1</sup> Xiao-Xia Cai,<sup>1</sup> Jun Zhou,<sup>4</sup> Ming Gong,<sup>5</sup> Zhao-Feng Liu,<sup>5</sup> Shuang-Yu Zheng,<sup>4</sup> Deng-Ke Ma,<sup>4</sup> Mo Chen,<sup>1</sup> Wei-Jie Sun,<sup>1</sup> Shuang Yang,<sup>1</sup> Fei Yan,<sup>1</sup> Yi-Rong Jin,<sup>1</sup> Xue-Feng Ding,<sup>5,†</sup> and Hai-Feng Yu<sup>1,6,‡</sup>

<sup>1</sup>*Beijing Academy of Quantum Information Sciences, Beijing, 100193, China*

<sup>2</sup>*The Institute of Physics, Chinese Academy of Sciences, Beijing, 100190, China*

<sup>3</sup>*University of Chinese Academy of Sciences, Beijing, 101408, China*

<sup>4</sup>*School of Physics and Technology, Nanjing Normal University, Nanjing 210023, China*

<sup>5</sup>*Institute of High Energy Physics, Chinese Academy of Sciences, Beijing, 100049, China*

<sup>6</sup>*Hefei National Laboratory, Hefei 230088, China*

(Dated: February 7, 2024)

Correlated errors can significantly impact the quantum error correction, which challenges the assumption that errors occur in different qubits independently in both space and time. Superconducting qubits have been found to suffer correlated errors across multiple qubits, which could be attributable to ionizing radiations and cosmic rays. Nevertheless, the direct evidence and a quantitative understanding of this relationship are currently lacking. In this work, we propose to continuously monitor multi-qubit simultaneous charge-parity jumps to detect correlated errors and find that occur more frequently than multi-qubit simultaneous bit flips. Then, we propose to position two cosmic-ray muon detectors directly beneath the sample box in a dilution refrigerator and successfully observe the correlated errors in a superconducting qubit array triggered by muons. By introducing a lead shielding layer on the refrigerator, we also reveal that the majority of other correlated errors are primarily induced by gamma rays. Furthermore, we find the superconducting film with a higher recombination rate of quasiparticles used in the qubits is helpful in reducing the duration of correlated errors. Our results provide experimental evidence of the impact of gamma rays and muons on superconducting quantum computation and offer practical insights into mitigation strategies for quantum error correction. In addition, we observe the average occurrence rate of muon-induced correlated errors in our processor is approximately  $0.40 \text{ min}^{-1}\text{cm}^{-2}$ , which is comparable to the muon event rate detected by the muon detector with  $0.506 \text{ min}^{-1}\text{cm}^{-2}$ . This demonstrates the potential applications of superconducting qubit arrays as low-energy threshold sensors in the field of high-energy physics.

## I. INTRODUCTION

Quantum bits (qubits) are inherently susceptible to various types of errors, necessitating the implementation of quantum error correction to build logical qubits for the realization of fault-tolerant quantum computer [1, 2]. The surface code is one of the promising fault-tolerance error correction schemes that leverages the topological properties of a qubit system to tolerate arbitrary local errors [3]. The presence of non-local correlated errors can disrupt the topological properties, thereby posing challenges to quantum error correction [4–6]. Although small-scale multi-qubit correlated errors can be alleviated by the optimization of error correction methods or the allocation of more physical qubits [7, 8], the effectiveness of these strategies diminishes when faced with large-scale correlated errors, thus constituting a significant challenge to overcome.

The correlated errors, such as offset-charge jump and energy relaxation, have been observed in superconducting qubits, and through the numerical simulation, it is explained such errors may arise from the quasiparticles (QPs) bursts induced by the high-energy particles, such as gamma rays or cosmic-ray muons [9, 10]. The large-scale correlated errors in a superconducting qubit array, by monitoring multi-qubit simultaneous energy relaxations, have also been observed in the Google Sycamore quantum processor [11]. In addition, Ref. [12] has experimentally demonstrated the impact of ion-

izing radiations on a superconducting qubit which can limit the qubit coherence time to milliseconds. These works suggest the correlated errors may be caused by gamma rays and muons, but direct experimental evidence is still lacking. To mitigate such errors, it is also imperative to provide a detailed understanding of their impact on the superconducting quantum processor.

In this work, we observe strong coincidences between correlated errors in a superconducting qubit array and muon events, thus providing direct experimental evidence of correlated errors induced by muons. The detection of correlated errors involves the continuous monitoring of multi-qubit correlated charge-parity jumps or bit flips, while muon events are identified through two muon detectors positioned directly beneath the sample box in a dilution refrigerator. After shielding the dilution refrigerator with a lead (Pb) shield, we observe a nearly identical reduction rate between QPs bursts and events detected by a gamma-ray detector, indicating the other major source of QPs bursts is induced by gamma rays. Then, we analyze the muon-induced QPs bursts and provide a detailed dynamic process of QPs bursts, finding that the QPs burst relaxed much faster in our processor compared to the Google Sycamore processor [11]. We attribute this to the rapid recombination rate of the QPs in the superconducting tantalum film of our processor. This can also potentially explain the little impact of radiation on the 27-qubit IBM Quantum Falcon R6 processor [13]. Therefore, our discovery provides

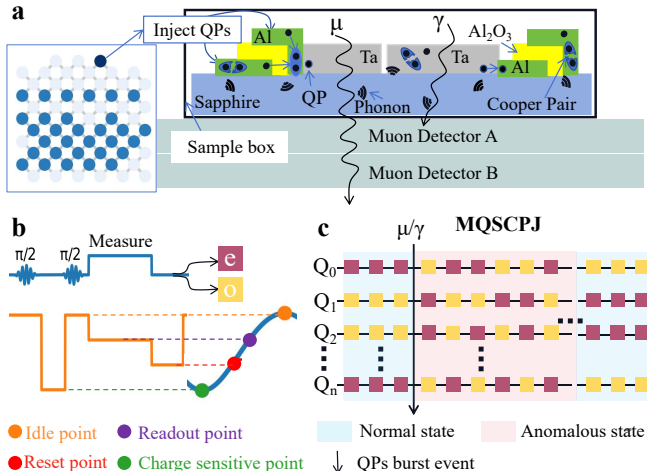


**FIG. 1: The generation process and detecting method of quasi-particles (QPs) burst.** (a) The non-equilibrium phonons can induce QPs bursts by Cooper pairs broken. These phonons are generated through the recombination of injected QPs, or the energy deposition in sapphire from high-energy particles such as muons ( $\mu$ ) and gamma ( $\gamma$ ) rays. Two muon detectors, named MDA and MDB, are positioned at the base of the sample box to identify muons that traverse both the sapphire and the muon detector concurrently. Our device consists of a square lattice with 63 flipmon qubits (circles) and 105 couplers (strips), and we select 31 qubits (blue circles) for our experiments. The dark blue qubit is intentionally utilized to inject QPs. (b) The measurement sequence to determine the charge-parity jump of the qubit. The qubit frequency is biased to the idle point, readout point, reset point, or charge-sensitive point, as guided by the dashed lines on the spectrum (blue line) of the qubit, for state control, measurement, initialization, or charge parity detection, respectively. (c) The schematic of one typical QPs burst. We continuously monitor charge-parity jumps of all selected qubits in a period of 5.6  $\mu$ s. The QPs burst induced by  $\mu$  or  $\gamma$  is identified when there is a multi-qubit simultaneous charge-parity jump (MQSCPJ).

an additional solution, to mitigate such correlated errors, by considering the choice of superconducting material of qubit. Furthermore, we find our quantum processor using the proposed QPs burst method exhibits a high muon detection rate, suggesting the potentially superior performance in low-energy particle detection [14, 15].

## II. RESULTS

### A. Device and QPs bursts detection

The phenomenological picture of the generation process with correlated errors in superconducting qubits is illustrated in Fig. 1a. A high-energy particle traverses the sapphire substrate, deposits a large amount of energy, and generates numerous phonons. These non-equilibrium phonons can propagate throughout the entire substrate, creating excessive QPs in superconducting films through the Cooper pairs broken. Subsequently, the tunnelings of these QPs across the Josephson junctions can affect the energy relaxations and dephasings of

the qubits [16–18] and thus induce the correlated errors in superconducting qubits. Two muon detectors are positioned close to each other, directly under the sample box in our refrigerator at approximately 14 mK. Therefore, we can pinpoint almost all the occurrences of a muon passing through the qubit substrate.

To detect a QPs burst, it is essential to continuously measure the correlated errors at very short intervals in a large qubit array. We select 31 well-behaved qubits to form a superconducting qubit array in a quantum processor similar to the one described in Ref. [19], where each flipmon qubit [20] is composed of tantalum capacitor pads, indium bump, and aluminum Josephson junctions. We use the appropriate asymmetrical design for qubit junctions to realize the qubit spectrum featuring two sweet spots and spanning from 2.97 GHz to 7.13 GHz, shown in Fig. 1b. To achieve rapid correlated error measurements, a crucial factor is the implementation of a fast qubit reset. In this setup, the frequency of the readout resonators is set at approximately 4.33 GHz. This enables us to tune the qubit frequency to match the readout resonator frequency, thereby fast resetting the qubit to  $|0\rangle$  state.

We perform the single qubit gate at the idle point (high sweet spot) and optimize the qubit frequency during qubit measurement to enhance readout fidelity. At the low sweet spot, the qubit exhibits a charge-sensitive point in the ratio of Josephson energy and charging energy  $E_J/E_C \approx 16$  [21]. This leads to the significantly distinct qubit frequencies at the even and odd charge of the qubit island. We can measure this charge parity by employing a Ramsey-based sequence shown in Fig. 1b. We first initialize the qubit at the superposition state  $(|0\rangle + |1\rangle)/\sqrt{2}$  by applying a  $\pi/2$  pulse, followed by a short idle time at the low sweet spot to accumulate a  $\pi$  phase difference between even and odd charge parity. Subsequently, a second  $\pi/2$  pulse is applied to map the charge-parity state ( $|e\rangle$  or  $|o\rangle$ ) into the qubit state ( $|1\rangle$  or  $|0\rangle$ ) [22]. Finally, we can measure the qubit state to obtain the charge-parity state.

Ref. [11] has demonstrated the QPs bursts could be identified by continuously monitoring multi-qubit simultaneous bit flips (defined as  $|1\rangle$  state flip to  $|0\rangle$  state) (MQSBF). Here we note that the sensitivity of qubit charge-parity jumps to QPs tunneling exceeds that of qubit bit flips [22, 23]. In this context, we propose continuously monitoring multi-qubit simultaneous charge-parity jumps (MQSCPJ) to identify QPs bursts. As illustrated in Fig. 1c, we repeat the charge-parity measurement sequence across all selected qubits with a period of 5.6  $\mu$ s. The initial parity state of each qubit is random but stabilizes during subsequent measurements, indicated as the normal state. However, when a QPs burst occurs, charge-parity jumps across numerous qubits are observed, which are indicated as the anomalous state. After the relaxation of the QPs burst is finished, each qubit would go back to the normal state, where all qubits exhibit a stable parity state during measurements.

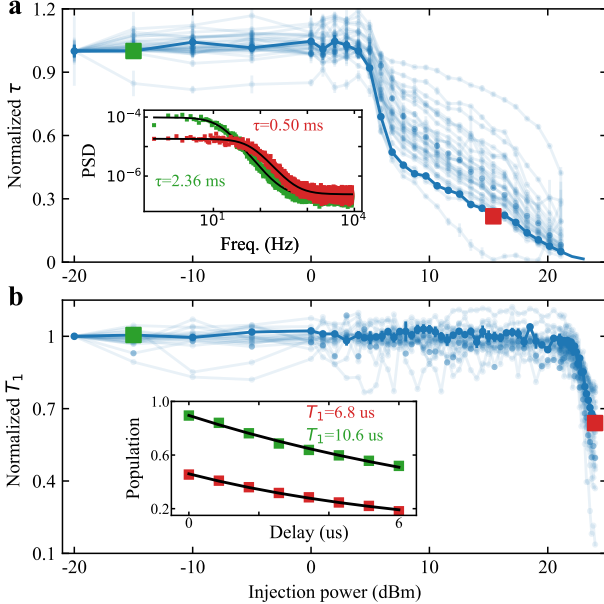


FIG. 2: **Sensitivity of the charge-parity jump and bit flip to the QPs density.** (a),(b) The normalized characteristic time of charge-parity jump ( $\tau$ ) and bit flip ( $T_1$ ) as a function of QPs injection power for different qubits. The QPs density can be increased by increasing the injection power. The selected typical curve of one qubit is shown in the dark blue line for clarity. Inset: the power spectral density (PSD) of the QPs tunneling and population decay are fitted to give the  $\tau$  and  $T_1$ , which is represented by orange and red squares in (a) and (b), respectively.

### B. The sensitivity of two detection methods

We first experimentally evaluate the sensitivity of the charge-parity jump and bit flip to the QP density. To vary the QPs density, we select a qubit to inject QPs, shown in Fig. 1a [24]. We apply a strong microwave pulse to the readout resonator of the injected qubit, generating an oscillating voltage across the Josephson junction. When the voltage exceeds the aluminum superconducting Josephson junction gap of about 180  $\mu$ eV, a large number of QPs can be generated on each island of the injected qubit. The recombination of these QPs will produce numerous phonons, which subsequently propagate throughout the substrate, and then create a large number of QPs for many qubits. Following this, we can change the QP density of each qubit by modifying the injection power.

For each QP density, we measure the characteristic time of charge-parity jumps ( $\tau$ ) and bit flips ( $T_1$ ). The time evolution of charge parity can be modeled as a symmetric random telegraph signal and thus we can determine  $\tau$  by analyzing their power spectral density [25]. As an example, shown in the inset of Fig. 2a,  $\tau$  is 2.36 ms at an injection power of -15 dBm and 0.5 ms at 15.4 dBm.  $T_1$  can be determined by conducting the population decay experiment, shown in the inset of Fig. 2b with  $T_1 = 10.6$   $\mu$ s and 6.8  $\mu$ s at injection powers of -15 dBm and 24 dBm, respectively. Figs. 2a and 2b display the

normalized characteristic times as  $\tau/\tau(-20\text{dBm})$  and  $T_1/T_1(-20\text{dBm})$  for multiple qubits as a function of injection power, respectively. The dark blue lines represent typical curves. Especially in Fig. 2a, it illustrates the distinctive feature of the QPs excitation in the superconductor as a function of the injection power [26, 27]. We find the  $T_1$  for each qubit remains unchanged until the injection power reaches approximately 22 dBm, however, the  $\tau$  undergoes a noticeable change at an injection power of around 5 dBm. This does indicate the charge-parity jump is significantly more sensitive to QP density than bit flip.

### C. Experimental evidence of QPs bursts induced by muons

Reference [9] conducted a numerical simulation of the QPs burst using the GEANT4 toolkit [28] and attributed the origin of these events to gamma rays and cosmic-ray muons. To experimentally verify this, we propose to directly observe the coincidences between QPs bursts and the muon events. The key point in our experiment is to install two homemade muon detectors, namely MDA and MDB, directly beneath the sample box inside the refrigerator, as described in Fig. 1a. Employing two muon detectors makes it possible to distinguish signals caused by gamma rays, as such rays are less likely to produce simultaneous responses on both detectors, a criterion we have defined as muon events. Each muon detector is composed of a plastic scintillator serving as the detection medium, along with a silicon photo-multiplier tube for signal collection. After the amplification at room temperature, the signal can be captured in a continuous acquisition mode by a data acquisition card [25].

The QPs bursts can be detected by continuously monitoring MQSCPJ and MQSBF. However, the limited operation fidelity of the qubit generates background noise. For the MQSCPJ experiment, we smooth the continuous-monitored charge-parity data for each qubit through convolution with a squared window in the length of 20 sampling points. Subsequently, we calculate the charge-parity jump probability for each qubit and average these probabilities across all the selected qubits, defining it as the smoothed MQSCPJ rate. For the MQSBF experiment, we calculate the ratio of the number of error qubits to the total number of selected qubits and convolve it with a Gaussian window in the length of 40 sampling points, defined as the MQSBF rate. Ultimately, we can employ these two methods as two QPs burst detectors [25].

Once the time delay between the MQSCPJ or MQSBF detector and two muon detectors is calibrated, we can turn on these detectors simultaneously and begin data acquisition. In Fig. 3a, we show the typical time series of continuously monitoring the smoothed MQSCPJ rate. The numerous anomalous peaks (orange dots) are identifiable, deviating significantly from the background noise, indicating the presence of the QPs burst in our quantum processor. We observe 41 QPs bursts and 127 muon events in a duration of 598 s. A representative time slice of a single muon event with a time resolution of

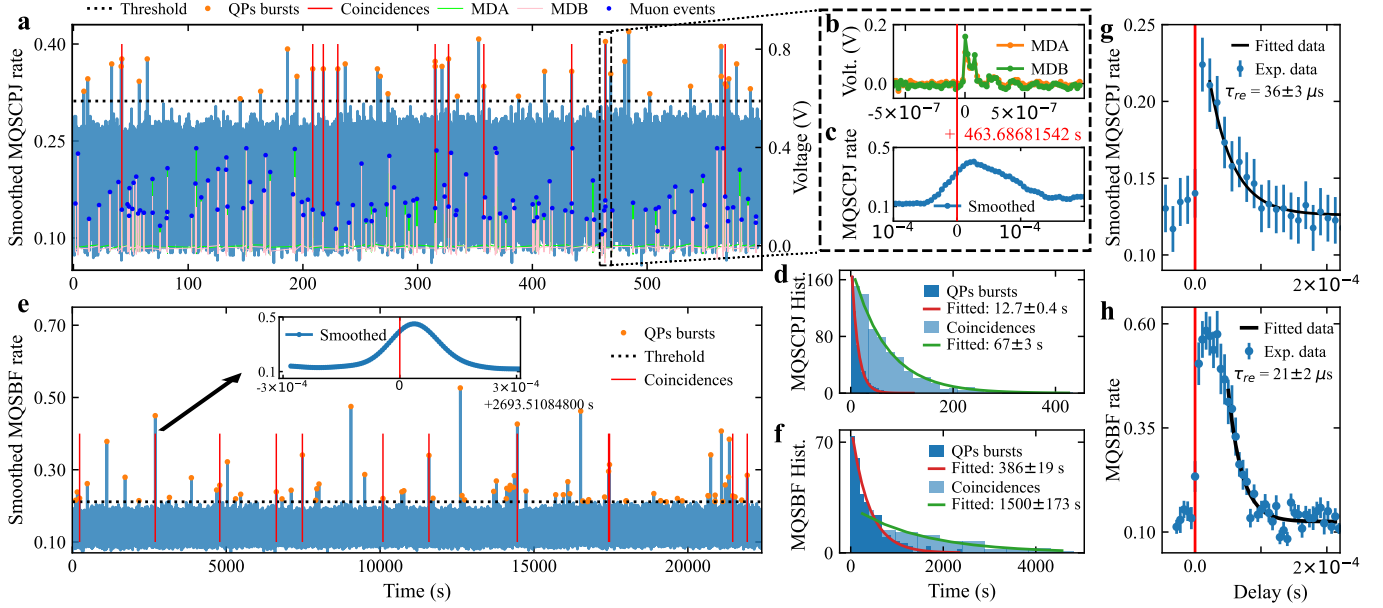


FIG. 3: **The coincidence experiment.** (a) The time series of continuously monitoring the smoothed rates of multi-qubit simultaneous charge-parity jump (the blue line) to observe the coincidences between QPs bursts and muon events over durations of 598 s. The selected peaks (orange dots) are identified as the QPs burst with the threshold 0.31 shown in black dashed lines. In (a), we detect 41 QPs bursts and 127 muon events (blue dots). The independent random coincidence rate is extremely low, however, 10 coincident events are identified here. (b), (c) Time-slices of a typical coincidence event. The voltage of MDA and MDB displaying the peak simultaneously is identified as a muon event. The red line indicates the coincidence moment. (d) The histograms of the time intervals between neighboring coincidence events for MQSCPJ experiments. The blue and light blue bars represent all QPs bursts and coincidence events, respectively. This histogram obeys exponential distribution and can be fitted to give the average event occurring time, respectively. (e) Similar with (a), The smoothed rates of multi-qubit simultaneous bit flip (MQSBF) are monitored over 22399 s with a threshold of 0.18. 75 QPs bursts, 4751 muon events (not shown), and 12 coincident events are detected. Inset of (e): similar with (c), except that we only record the timestamp of the muon events. (f) Similar to (d), The histograms of MQSBF experiments also give the average event occurring time of all QPs bursts and coincidence events. (g), (h) As for coincidence events, by setting the muon events as the trigger events shown in red solid lines, we can obtain the average dynamic processes of the MQSCPJ and MQSBF rates shown in blue dots. Black lines are the exponential fitted data and thus yield the recombination time ( $\tau_{re}$ ) with  $36 \pm 3 \mu\text{s}$  and  $21 \pm 2 \mu\text{s}$ , respectively. To better describe this rapid process, the length of the smoothing window used in (g) is only 2 sampling points, while no smoothing window is used in (h).

20 ns is shown in Fig. 3b. We identify the coincidences between QPs bursts and muon events by confirming both peaks of the events fall within the time window of 100  $\mu\text{s}$ , shown in Figs. 3b and 3c. Since the signal of the QPs burst appears wider after smoothing, this does not necessarily mean that the QPs burst precedes the occurrence of muon events. If the QPs bursts and muon events are completely uncorrelated, the probability of one coincidence within the duration of 598 s is  $(41 \times 127)/(598 \text{ s}/100 \mu\text{s}) \approx 8.7 \times 10^{-4}$  [25]. However, 10 coincident events are identified, as indicated by the red solid lines, thus providing direct experimental evidence of these QPs bursts being induced by the muon events. In addition, we repeat the MQSCPJ experiments and exponentially fit the histograms of the time intervals between neighboring events to yield the average occurrence times of  $12.7 \pm 0.4$  s for all QPs bursts,  $67 \pm 3$  s for muon-induced QPs bursts, shown in Fig. 3d. Taking into account the size of our qubit chip (15mm  $\times$  15mm), we can calculate a coincidence occurrence rate of  $0.40 \pm 0.02 \text{ min}^{-1} \text{cm}^{-2}$ . The contribution of the carrier chip to the coincidence occurrence rate requires further investigation.

Correlated bit-flip errors exert a more big influence on the quantum error correction in superconducting qubits [9, 10]. Here we also perform the MQSBF experiment, and record 75 QPs bursts and 4751 muon events in a duration of 22399 s, shown in Fig. 3e. We only capture the timestamps of muon events to minimize data storage requirements in long-term MQSBF experiments. As indicated by the red solid lines, 12 coincident events are also observed, whereas, the uncorrelated hypothesis gives the probability of one coincidence within the duration of 22399 s is  $1.6 \times 10^{-3}$ . This again confirms that the QPs bursts are induced by muon events. The repeated MQSBF experiments give the average occurrence times of  $386 \pm 19$  s for all QPs bursts,  $1500 \pm 173$  s for muon-induced QPs bursts, shown in Fig. 3f.

To resolve the dynamic behavior of the QPs bursts induced by muon events, we designate the muon events as the trigger event and average the corresponding coincident events, as shown in Figs. 3g and 3h. To describe this fast process in more detail, we employ a smoothing window with only 2 sampling points for the MQSCPJ experiment and avoid using the smoothing window for the MQSBF experiment. We fit the

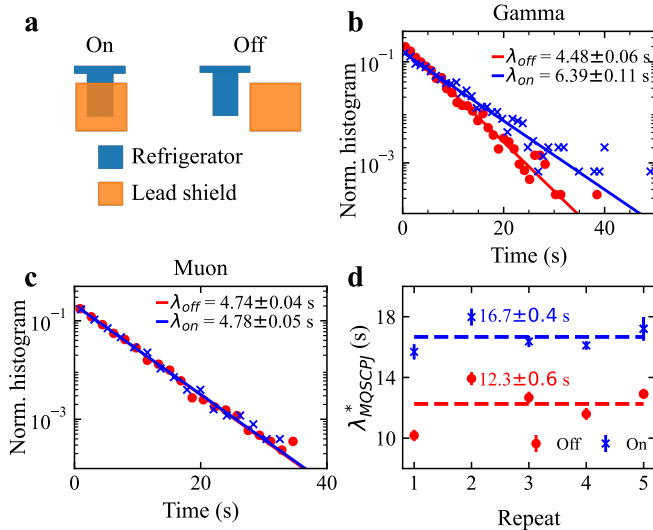


FIG. 4: **The shielding experiment.** (a) Schematic of the dilution refrigerator with ('On') and without ('Off') Lead shield. (b), (c) The normalized histograms of the time intervals between neighboring events of the gamma ray detector and muon detector with and without the Pb shield, named as shield on (cross dots) or off (circle dots). The solid lines in all graphs represent the exponential fitted data, respectively. (d) The QPs burst event occurring time is measured with shield and then without shield. This cycle is repeated 5 times to give an average value of  $16.7 \pm 0.4$  s ( $12.3 \pm 0.6$  s) for the shield on (off).

tail of the events and determine the recombination time to be  $36 \pm 3 \mu\text{s}$  and  $21 \pm 2 \mu\text{s}$ , respectively. This difference might be explained by the distinct sensitivity to the QPs tunneling between charge-parity jump and bit flip. To understand the physics in detail requires further exploration.

The recombination time is roughly two orders of magnitude faster than what has been observed in the Google Sycamore quantum processor [11]. This can be ascribed to the properties of the superconducting films, with the recombination rate of QPs in the Ta film of our qubit chip being two orders of magnitude faster than in the aluminum (Al) film of their qubit chip [29]. We can also potentially explain the lack of impact of cosmic rays on the 27-qubit IBM Quantum Falcon R6 processor [13], because they conduct the experiment at a lower time resolution of  $40 \mu\text{s}$  on qubits in a niobium (Nb) film which also exhibits a much faster recombination time (approximate several microseconds) of QPs [30]. This result also suggests that qubit superconducting films with a higher QP recombination rate can reduce the duration of the correlated errors.

#### D. The other sources of QPs burst

In addition to muon-induced QPs bursts in Figs. 3a and 3e, the other sources may be attributed to gamma rays originating from the environment. As illustrated in Fig. 4a, we employ a homemade Pb shield with a thickness of 1 cm on the dilution

refrigerator to reduce external gamma rays [25]. To evaluate the shielding effectiveness, we place a gamma detector inside the Pb shield at approximately the same location as the qubit chip in the above experiment. In Fig. 4b, we obtain an average occurrence time of  $4.48 \text{ s}$  ( $6.38 \text{ s}$ ) without (with) Pb shield, indicating a shielding efficiency of  $(6.38 - 4.48)/4.48 = 43\%$  with error-bar about 3%. However, it shows almost no effect on the muon events with an average occurrence time of  $4.74 \text{ s}$  ( $4.78 \text{ s}$ ) without (with) Pb shield, as depicted in Fig. 4c. Considering the size of the plastic scintillator with  $5 \text{ cm} \times 5 \text{ cm} \times 1 \text{ cm}$ , we calculate a muon detection rate of  $0.506 \pm 0.004 \text{ min}^{-1} \text{cm}^{-2}$ , which is approaching  $0.56 \text{ min}^{-1} \text{cm}^{-2}$  deduced by numerical simulation [25].

To eliminate random fluctuations, we monitor the MQSCPJ and collect hundreds of events with the shield off, followed by the shield on, and finally repeat this cycle five times. As shown in Fig. 4d, the average values are  $16.7 \pm 0.4 \text{ s}$  ( $12.3 \pm 0.6 \text{ s}$ ) with shield on (off), indicating the average occurrence time except for the muon-induced QPs bursts is  $1/(1/16.7 - 1/67) \text{ s} = 22.2 \text{ s}$  with shield on,  $1/(1/12.3 - 1/67) \text{ s} = 15.1 \text{ s}$  with shield off. Thus, the shielding efficiency detected by the MQSCPJ experiment is  $(22.2 - 15.1)/15.1 = 47\%$  with error-bar about 10%, which is close to the efficiency of 43% detected by the gamma detector. This suggests the QPs bursts induced by the other sources are mainly from the external gamma rays.

### III. DISCUSSION

We provide direct evidence that correlated errors in superconducting qubits are mainly induced by gamma rays and muons and resolve the impact of muons on a superconducting quantum processor. We find the correlated charge-parity jumps occur more frequently than the correlated bit flips. Such correlated errors not only pose a huge challenge to the superconducting quantum error correction but also have a big impact on topologically protected Majorana qubits [31–33]. Our result indicates serious attention must be paid to this issue in fault-tolerant quantum computation based on solid-state quantum systems.

In our superconducting quantum processor, the correlated errors occur at a rate of approximately  $1/(12.3 \text{ s})$ , which remains too high for the practical implementation of a quantum error correction. The most effective mitigation approach is to conduct the experiment deep underground [34, 35]. However, such an approach would result in a significantly high cost. On the ground, gamma rays can be easily shielded with Pb, but the effect of shielding muons is negligible. Our work indicates that the muon detector can operate within the dilution refrigerator, which enables us to develop a muon detection array for the identification of the occurrence and location of a muon-induced QPs burst. Thus we can employ it to execute another round of quantum error correction to correct such errors [36–38]. In addition, several methods have been proposed, such as using lower-gap superconductor or normal metal as the quasi-particle traps [26, 39] and phonon traps [40], and suppress-

ing the phonon transport [41] to mitigate the correlated errors on the chip. Here, our results also indicate the choice of the superconducting film material with stronger electron-phonon interaction which has a higher QPs recombination rate, leads to a shorter duration of correlated errors [30, 42].

Through the QPs injection experiment, we demonstrate the generated meV energy-level phonons can be detected by our proposed method. Meanwhile, our processor has also shown muon detection efficiency comparable to the muon detector. These findings indicate superconducting qubit array with our method can be used as a low-energy threshold particle detector, such as meV phonon, and THz photon and thus show the potential applications in detecting low-mass dark matter and cosmic microwave background radiation. [14, 15, 43, 44].

We appreciate the helpful discussion with Prof. T. Xiang. We thank X. Liang, C. Yang, C. Wang, T. Su, C. Li, and Z. Mi for their work on the quantum chip preparation. We acknowledge support from the National Natural Science Foundation of China (Grant Nos. 11890704, 12104055, 92365206, 22303005, 12275133, and E311455C), Innovation Program for Quantum Science and Technology (No.2021ZD0301802) and Chinese Academy of Sciences Laboratory Innovation Fund E3291TD. M.G. and Z. L. acknowledge the support from the Innovative Projects of Science and Technology at IHEP,CAS.

### Competing interests

The authors declare no competing interests.

\* These authors contributed equally to this work.

† Electronic address: [dingxf@ihep.ac.cn](mailto:dingxf@ihep.ac.cn)

‡ Electronic address: [hfyu@baqis.ac.cn](mailto:hfyu@baqis.ac.cn)

- [1] D. Gottesman, “Theory of fault-tolerant quantum computation,” *Phys. Rev. A* **57**, 127–137 (1998).
- [2] P. Aliferis, D. Gottesman, and J. Preskill, “Quantum accuracy threshold for concatenated distance-3 codes,” [arXiv:quant-ph/0504218](https://arxiv.org/abs/quant-ph/0504218) (2005).
- [3] A. G. Fowler, M. Mariantoni, J. M. Martinis, and A. N. Cleland, “Surface codes: Towards practical large-scale quantum computation,” *Phys. Rev. A* **86** (2012).
- [4] A. G. Fowler and J. M. Martinis, “Quantifying the effects of local many-qubit errors and nonlocal two-qubit errors on the surface code,” *Phys. Rev. A* **89** (2014).
- [5] C. T. Chubb and S. T. Flammia, “Statistical mechanical models for quantum codes with correlated noise,” *Annales de l’Institut Henri Poincaré D* **8**, 269–321 (2021).
- [6] R. Harper and S. T. Flammia, “Learning correlated noise in a 39-qubit quantum processor,” *PRX Quantum* **4**, 040311 (2023).
- [7] A. G. Fowler, “Optimal complexity correction of correlated errors in the surface code,” [arXiv:1310.0863](https://arxiv.org/abs/1310.0863) (2013).
- [8] P. Baireuther, T. E. O’Brien, B. Tarasinski, and C. W. J. Beenakker, “Machine-learning-assisted correction of correlated qubit errors in a topological code,” *Quantum* **2**, 48 (2018).

- [9] C. D. Wilen, S. Abdullah, N. A. Kurinsky, C. Stanford, L. Cardani, G. D’Imperio, C. Tomei, L. Faoro, L. B. Ioffe, C. H. Liu, A. Opremcak, B. G. Christensen, J. L. DuBois, and R. McDermott, “Correlated charge noise and relaxation errors in superconducting qubits,” *Nature* **594**, 369–373 (2021).
- [10] J. M. Martinis, “Saving superconducting quantum processors from decay and correlated errors generated by gamma and cosmic rays,” *npj Quantum Information* **7**, 90 (2021).
- [11] M. McEwen, L. Faoro, K. Arya, A. Dunsworth, T. Huang, S. Kim, B. Burkett, A. Fowler, F. Arute, J. C. Bardin, A. Bengtsson, A. Bilmes, B. B. Buckley, N. Bushnell, Z. Chen, R. Collins, S. Demura, A. R. Derk, C. Erickson, M. Giustina, S. D. Harrington, S. Hong, E. Jeffrey, J. Kelly, P. V. Klimov, F. Kostritsa, P. Laptev, A. Locharla, X. Mi, K. C. Miao, S. Montazeri, J. Mutus, O. Naaman, M. Neeley, C. Neill, A. Opremcak, C. Quintana, N. Redd, P. Roushan, D. Sank, K. J. Satzinger, V. Shvarts, T. White, Z. J. Yao, P. Yeh, J. Yoo, Y. Chen, V. Smelyanskiy, J. M. Martinis, H. Neven, A. Megrant, L. Ioffe, and R. Barends, “Resolving catastrophic error bursts from cosmic rays in large arrays of superconducting qubits,” *Nature Physics* **18**, 107–111 (2021).
- [12] A. P. Vepsäläinen, A. H. Karamlou, J. L. Orrell, A. S. Dogra, B. Loer, F. Vasconcelos, D. K. Kim, A. J. Melville, B. M. Niedzielski, J. L. Yoder, S. Gustavsson, J. A. Formaggio, B. A. VanDevender, and W. D. Oliver, “Impact of ionizing radiation on superconducting qubit coherence,” *Nature* **584**, 551–556 (2020).
- [13] T. Thorbeck, A. Eddins, I. Lauer, D. T. McClure, and M. Carroll, “Two-level-system dynamics in a superconducting qubit due to background ionizing radiation,” *PRX Quantum* **4**, 020356 (2023).
- [14] A. Chou, K. Irwin, R. H. Maruyama, O. K. Baker, C. Bartram, K. K. Berggren, G. Cancelo, D. Carney, C. L. Chang, H.-M. Cho, *et al.*, “Quantum sensors for high energy physics,” [arXiv:2311.01930](https://arxiv.org/abs/2311.01930) (2023).
- [15] C. W. Fink, C. Salemi, B. A. Young, D. I. Schuster, and N. A. Kurinsky, “The superconducting quasiparticle-amplifying transmon: A qubit-based sensor for mev scale phonons and single thz photons,” [arXiv:2310.01345](https://arxiv.org/abs/2310.01345) (2023).
- [16] J. M. Martinis, M. Ansmann, and J. Aumentado, “Energy decay in superconducting josephson-junction qubits from nonequilibrium quasiparticle excitations,” *Phys. Rev. Lett.* **103**, 097002 (2009).
- [17] G. Catelani, S. E. Nigg, S. M. Girvin, R. J. Schoelkopf, and L. I. Glazman, “Decoherence of superconducting qubits caused by quasiparticle tunneling,” *Phys. Rev. B* **86**, 184514 (2012).
- [18] K. Serniak, M. Hays, G. de Lange, S. Diamond, S. Shankar, L. Burkhardt, L. Frunzio, M. Houzet, and M. Devoret, “Hot nonequilibrium quasiparticles in transmon qubits,” *Phys. Rev. Lett.* **121** (2018).
- [19] X.-G. Li, H.-K. Xu, J.-H. Wang, L.-Z. Tang, D.-W. Zhang, C.-H. Yang, T. Su, C.-L. Wang, Z.-Y. Mi, W.-J. Sun, X.-H. Liang, M. Chen, C.-Y. Li, Y.-S. Zhang, K.-H. Linghu, J.-X. Han, W.-Y. Liu, Y.-L. Feng, P. Liu, G.-M. Xue, J.-N. Zhang, Y.-R. Jin, S.-L. Zhu, H.-F. Yu, and Q.-K. Xue, “Mapping a topology-disorder phase diagram with a quantum simulator,” [arXiv:2301.12138](https://arxiv.org/abs/2301.12138) (2023).
- [20] X. Li, Y. Zhang, C. Yang, Z. Li, J. Wang, T. Su, M. Chen, Y. Li, C. Li, Z. Mi, X. Liang, C. Wang, Z. Yang, Y. Feng, K. Linghu, H. Xu, J. Han, W. Liu, P. Zhao, T. Ma, R. Wang, J. Zhang, Y. Song, P. Liu, Z. Wang, Z. Yang, G. Xue, Y. Jin, and H. Yu, “Vacuum-gap transmon qubits realized using flip-chip technology,” *Applied Physics Letters* **119** (2021).
- [21] J. Koch, T. M. Yu, J. Gambetta, A. A. Houck, D. I. Schuster,

J. Majer, A. Blais, M. H. Devoret, S. M. Girvin, and R. J. Schoelkopf, “Charge-insensitive qubit design derived from the cooper pair box,” *Phys. Rev. A* **76** (2007).

[22] D. Ristè, C. C. Bultink, M. J. Tiggelman, R. N. Schouten, K. W. Lehnert, and L. DiCarlo, “Millisecond charge-parity fluctuations and induced decoherence in a superconducting transmon qubit,” *Nature Communications* **4** (2013).

[23] J. Wenner, Y. Yin, E. Lucero, R. Barends, Y. Chen, B. Chiaro, J. Kelly, M. Lenander, M. Mariantoni, A. Megrant, C. Neill, P. J. J. O’Malley, D. Sank, A. Vainsencher, H. Wang, T. C. White, A. N. Cleland, and J. M. Martinis, “Excitation of superconducting qubits from hot nonequilibrium quasiparticles,” *Phys. Rev. Lett.* **110**, 150502 (2013).

[24] C. Wang, Y. Y. Gao, I. M. Pop, U. Vool, C. Axline, T. Brecht, R. W. Heeres, L. Frunzio, M. H. Devoret, G. Catelani, L. I. Glazman, and R. J. Schoelkopf, “Measurement and control of quasiparticle dynamics in a superconducting qubit,” *Nature Communications* **5** (2014).

[25] “More details can be found in the supplementary materials.”

[26] A. Bargerbos, L. J. Splitthoff, M. Pita-Vidal, J. J. Wesdorp, Y. Liu, P. Krogstrup, L. P. Kouwenhoven, C. K. Andersen, and L. Grünhaupt, “Mitigation of quasiparticle loss in superconducting qubits by phonon scattering,” *Phys. Rev. Appl.* **19** (2023).

[27] U. Patel, I. V. Pechenezhskiy, B. L. T. Plourde, M. G. Vavilov, and R. McDermott, “Phonon-mediated quasiparticle poisoning of superconducting microwave resonators,” *Phys. Rev. B* **96**, 220501 (2017).

[28] M. Kelsey, R. Agnese, Y. Alam, I. A. Langrudy, E. Azadbakht, D. Brandt, R. Bunker, B. Cabrera, Y.-Y. Chang, H. Coombes, *et al.*, “G4cmp: Condensed matter physics simulation using the geant4 toolkit,” *Nuclear Instruments and Methods in Physics Research Section A: Accelerators, Spectrometers, Detectors and Associated Equipment* **1055**, 168473 (2023).

[29] R. Barends, S. van Vliet, J. J. A. Baselmans, S. J. C. Yates, J. R. Gao, and T. M. Klapwijk, “Enhancement of quasiparticle recombination in ta and al superconductors by implantation of magnetic and nonmagnetic atoms,” *Phys. Rev. B* **79** (2009).

[30] R. Gaitskell and J. Gaitskell, *Non-equilibrium superconductivity in niobium and its application to particle detection*, Ph.D. thesis, University of Oxford (1993).

[31] S. Albrecht, E. Hansen, A. Higginbotham, F. Kuemmeth, T. Jespersen, J. Nygård, P. Krogstrup, J. Danon, K. Flensberg, and C. Marcus, “Transport signatures of quasiparticle poisoning in a majorana island,” *Phys. Rev. Lett.* **118** (2017).

[32] V. Lahtinen and J. Pachos, “A short introduction to topological quantum computation,” *SciPost Physics* **3** (2017).

[33] X. Sun, Z. Lyu, E. Zhuo, B. Li, Z. Ji, J. Fan, X. Song, F. Qu, G. Liu, J. Shen, and L. Lu, “Quasiparticle poisoning rate in a superconducting transmon qubit involving majorana zero modes,” *arXiv:2211.08094* (2022).

[34] L. Cardani, F. Valenti, N. Casali, G. Catelani, T. Charpentier, M. Clemenza, I. Colantoni, A. Cruciani, G. D’Imperio, L. Gironi, L. Grünhaupt, D. Gusekova, F. Henriques, M. Lagoin, M. Martínez, G. Pettinari, C. Rusconi, O. Sander, C. Tomei, A. V. Ustinov, M. Weber, W. Wernsdorfer, M. Vignati, S. Pirro, and I. M. Pop, “Reducing the impact of radioactivity on quantum circuits in a deep-underground facility,” *Nature Communications* **12** (2021).

[35] E. Bertoldo, M. Martínez, B. Nedyalkov, and P. Forn-Díaz, “Cosmic muon flux attenuation methods for superconducting qubit experiments,” *arXiv:2303.04938* (2023).

[36] J. L. Orrell and B. Loer, “Sensor-assisted fault mitigation in quantum computation,” *Phys. Rev. Appl.* **16** (2021).

[37] Q. Xu, A. Seif, H. Yan, N. Mannucci, B. O. Sane, R. Van Meter, A. N. Cleland, and L. Jiang, “Distributed quantum error correction for chip-level catastrophic errors,” *Phys. Rev. Lett.* **129** (2022).

[38] J. L. Orrell and B. Loer, “Sensor-assisted fault mitigation in quantum computation,” *Phys. Rev. Appl.* **16**, 024025 (2021).

[39] U. Patel, I. V. Pechenezhskiy, B. L. T. Plourde, M. G. Vavilov, and R. McDermott, “Phonon-mediated quasiparticle poisoning of superconducting microwave resonators,” *Phys. Rev. B* **96** (2017).

[40] F. Henriques, F. Valenti, T. Charpentier, M. Lagoin, C. Gouriou, M. Martínez, L. Cardani, M. Vignati, L. Grünhaupt, D. Gusekova, J. Ferrero, S. T. Skacel, W. Wernsdorfer, A. V. Ustinov, G. Catelani, O. Sander, and I. M. Pop, “Phonon traps reduce the quasiparticle density in superconducting circuits,” *Applied Physics Letters* **115** (2019).

[41] V. Iaia, J. Ku, A. Ballard, C. P. Larson, E. Yelton, C. H. Liu, S. Patel, R. McDermott, and B. L. T. Plourde, “Phonon downconversion to suppress correlated errors in superconducting qubits,” *Nature Communications* **13** (2022).

[42] S. B. Kaplan, C. C. Chi, D. N. Langenberg, J. J. Chang, S. Jafarey, and D. J. Scalapino, “Quasiparticle and phonon lifetimes in superconductors,” *Phys. Rev. B* **14**, 4854 (1976).

[43] A. Das, N. Kurinsky, and R. K. Leane, “Dark matter induced power in quantum devices,” *arXiv:2210.09313* (2022).

[44] Y. Hochberg, E. D. Kramer, N. Kurinsky, and B. V. Lehmann, “Directional detection of light dark matter in superconductors,” *Phys. Rev. D* **107**, 076015 (2023).